Homeostatic normalization of sensory gain in auditory corticofugal feedback neurons

Meenakshi M Asokan[1,2*], Ross S Williamson[1,3], Kenneth E Hancock[1,2,3], and Daniel B Polley[1,2,3]

[1]Eaton-Peabody Laboratories, Massachusetts Eye and Ear Infirmary, Boston MA 02114

[2]Speech and Hearing Bioscience and Technology Program, Harvard Medical School, Boston MA 02115

[3]Department of Otolaryngology, Harvard Medical School, Boston MA 02114

[*]For correspondence: masokan@g.harvard.edu;

Keywords: Top-down, centrifugal, descending, feedback, tinnitus, hyperacusis, inferior colliculus, auditory cortex, GCaMP, homeostatic plasticity

Abstract

Sensory corticofugal neurons regulate gain and guide adaptive plasticity supporting innate and learned behaviors through their massive, widespread projections to subcortical sensory and motor nuclei. Little is known about the intrinsic, naturally occurring plasticity within corticofugal feedback neurons themselves, due to technical challenges associated with targeted long-term recordings from distributed deep layer cortical neurons. Here, we describe a chronic widefield Ca^{2+} axon imaging approach to track day-by-day dynamics in auditory corticocollicular (CCol) sound processing following auditory deprivation in adult mice. CCol responses were suppressed immediately following noise damage but rapidly returned to baseline levels despite ongoing elevation of cochlear thresholds. CCol response gain was potentiated for several days before stabilizing at baseline levels within six days after noise damage. These findings demonstrate a homeostatic plasticity in auditory corticofugal neurons that compensates both for a temporary elevation of cochlear thresholds and a permanent loss of cochlear afferent synapses.

Introduction

From the faint rustling of leaves to the blare of a trumpet, the auditory system encodes signal energies varying over a million-million fold (120 dB). The auditory system has evolved a host of mechanisms to compress this vast range of input signal energy into a dynamic range that can be encoded by cochlear electrochemical signaling with minimal wear and tear on the auditory transduction machinery. For example, parallel loops of brainstem efferent reflex pathways activate within milliseconds of intense noise to change the acoustic impedance of the middle ear and dampen excitability of cochlear sound transduction[1]. Central auditory circuits feature additional gain control mechanisms that rapidly optimize the dynamic range of neural encoding according to shifts in the signal-to-noise ratio of ambient sounds[2,3].

In addition to these "fast acting" gain control systems that operate on time scales of milliseconds to seconds, central auditory neurons are equipped with homeostatic gain control mechanisms that regulate neural excitability over time scales ranging from hours to days[4]. Damage to cochlear hair cells or auditory nerve fibers produces a sharp reduction in sound-evoked afferent signals conveyed from the inner ear to the brain. At all stages along the central auditory pathway, neurons compensate for a drop in afferent input through a spectrum of mechanisms including changes in intrinsic excitability[5,6], presynaptic neurotransmitter release properties[7,8], and shifts in the level and subunit composition of postsynaptic inhibitory and excitatory neurotransmitter receptors[9–13]. Collectively, these mechanisms increase the "central gain" on diminished bottom-up inputs from the damaged auditory periphery to drive overall activity levels back towards baseline homeostatic set points[14,15].

The auditory system features a massive set of centrifugal efferent projections that innervate a wide range of peripheral and central targets. Efferent olivocochlear and middle ear reflex pathways have a well-established role in rapid gain adjustment to protect the inner ear from injury and normalize activity levels in the auditory nerve[1,16]. A separate set of efferent centrifugal projections originate in the auditory cortex (ACtx) and innervate nearly all levels of subcortical auditory processing, including the thalamus, inferior colliculus (IC), superior olivary complex, and cochlear nucleus[17–19]. Compared with the olivocochlear efferent pathway, less is known about how corticofugal neurons contribute either to rapid gain control or slower, homeostatic normalization of neuronal excitability after auditory deprivation[16,20]. Prior studies have described striking short-term changes in subcortical gain control and sensory tuning resulting from non-selective lesions, inactivation or stimulation of ACtx neurons, but subcortical effects are often heterogeneous, with neurons in the same brain region showing diverse forms of modulation[21–25].

Corticofugal cell bodies are found in the deep layers of ACtx, interspersed among interneurons, ipsilateral and contralateral intratelencephalic projection neurons. Corticofugal neurons themselves are not a singular cortical cell type, but rather comprise a diverse set of projection neurons with distinct local inputs, subcortical targets, intrinsic properties and synaptic properties[26–31]. Traditional approaches to characterize the effects of cortical feedback on subcortical sound processing and plasticity through cooling, pharmacological silencing or microstimulation indiscriminately manipulate multiple types of corticofugal neurons as well as interneurons, intratelencephalic projection neurons or even axons of passage. This technical limitation likely explains why the subcortical effects of ACtx manipulations are often

heterogeneous and has generally hampered progress in understanding how corticofugal neurons contribute to auditory processing and perception. Recent efforts have begun to circumvent these limitations by using approaches to lesion[32,33], rewire[34], or optogenetically activate and inactivate[35–38] select classes of auditory projection neurons. Although paradigms to artificially manipulate the activity of corticofugal pathways have their appeal, there is also a need to selectively monitor the activity of these neurons and describe how naturally occurring plasticity in their auditory response profiles enable gain adjustments across a variety of time scales. To this end, we used a paradigm for chronic measurements of population sound-evoked activity in CCol axon terminals. We present here a single set of experiments that describe a homeostatic plasticity in the descending projections from the ACtx to the IC that increases central gain to compensate for temporary and permanent shifts in afferent drive from the cochlea over a time scale of several days.

Results

Visualizing sound-evoked activity from CCol neurons

To visualize sound-evoked activity in CCol neurons, we used a viral construct to express the genetically encoded calcium indicator, GCaMP6s (**Fig. 1A**). This construct induced widespread expression of GCaMP6s in ACtx neurons, with particularly concentrated expression in L5 (**Fig. 1B,** left). Projections of transduced ACtx neurons can be seen in the cortical white matter where some form a dense plexus of axon terminal fields in the dorsal and external cortex of the IC (Fig. 1B, white arrowhead), others innervate the auditory brainstem (Fig. 1B,

gray arrowhead) and still others innervate the contralateral auditory cortex, striatum, medial geniculate body and other subcortical targets not studied here.

In mice, the dorsal cap of the IC is a surface brain structure, providing us with the opportunity to make isolated measurements of CCol neurons by imaging sound-evoked activity from their axon terminals on the surface of the brain[39]. To this end, we developed a preparation to perform daily widefield imaging of sound-evoked activity from populations of CCol axons in awake, head-fixed mice (**Fig. 1C**). The dorsal surface of the IC and cerebellum are visible through the implanted cranial glass window, with CCol axon innervation clearly demarcating the boundaries of the IC under epifluorescent illumination (**Fig. 1D**).

Sound-evoked population CCol axon responses were sluggish, as expected from the GCaMP6s indicator, but grew reliably with the intensity of brief broadband noise bursts presented to the contralateral ear (**Fig. 1E**)[39–41]. By contrast, no measureable signals could be found in a similarly sized region of interest positioned over the cerebellum (**Fig. 1F**). We quantified the mean sound-evoked response amplitude across trials by expressing the difference between the post-stimulus peak and the mean of the pre-stimulus baseline period. Using this approach, we confirmed that CCol responses grew monotonically with stimulus intensity without any non-specific effects or stimulus-locked intrinsic signals in brain areas that did not express GCaMP6s (**Fig. 1G**).

Temporary and lasting inner ear damage following moderate intensity noise exposure

A sudden and selective loss of primary cochlear afferent neurons causes a paradoxical increase in the growth of sound-evoked activity in the ACtx and, to a lesser extent, the IC[42]. To

understand how CCol feedback was impacted by damage to cochlear afferent neurons, we implemented a protocol to track changes in the auditory brainstem response (ABR) and a non-invasive measure of outer hair cell function, the distortion product otoacoustic emission (DPOAE), following noise exposure that was calibrated to damage cochlear afferent synapses at the high-frequency base of the cochlea without causing permanent damage to cochlear hair cells (**Fig. 2A**)[43]. Following two days of baseline measurements, mice were exposed to a continuous band of octave-wide noise for 2 hours (**Fig. 2B**). As described in many previous studies in CBA/CaJ mice, this moderate intensity noise exposure was calibrated to cause a temporary shift in DPOAE and ABR thresholds immediately after noise exposure before returning to baseline levels (Repeated measures ANOVA, $F > 24$, $p < 0.0001$ for both DPOAE and ABR threshold shift at Day 1 versus 2 weeks, **Fig. 2C and Fig. 2D**, respectively)[44].

Wave 1 of the ABR is generated by Type-I spiral ganglion neurons, where the amplitude is proportional to the number of their intact synapses onto inner hair cells[45,46]. Prior work has demonstrated that a reduced amplitude of ABR wave 1 amplitude can reflect a "hidden" degeneration of primary cochlear afferents that is not detected by standard measurements of DPOAE and ABR threshold shift[44]. We confirmed this observation in our data; one day following noise exposure, ABR wave 1 amplitude was reduced at test frequencies ranging from 11.3 – 32 kHz (Repeated Measures ANOVA, Baseline vs. Day 1, $F > 12$, $p < 0.005$ for all 11.3-32 kHz; **Fig. 2E**). When measured again 2 weeks after noise exposure, a full recovery was observed at low- and mid-frequencies, yet wave 1 amplitudes remained significantly reduced at 22.6 and 32 kHz, presumably reflecting the permanent loss of cochlear afferent synapses at the high-frequency cochlear base (Repeated Measures ANOVA, Baseline vs. 2 weeks, $F < 2.1$, $p > 0.05$ for 8-16 kHz;

$F > 9$, $p < 0.005$ for 22.6 and 32 kHz). This hearing loss protocol allowed us to image sound-evoked CCol responses at three phases: *i*) during several days of a stable baseline period, *ii*) during a brief period of elevated thresholds immediately following noise exposure, and *iii*) during a period with normal cochlear thresholds but a permanent loss of cochlear afferent synapses.

Transient changes in CCol gain following noise exposure

We tracked daily changes in the growth of CCol population responses with sound intensity and observed a repeatable pattern of reduction, overshoot and stabilization following hearing loss. Looking at sound level growth functions from an example mouse, we observed stable monotonic responses in the two baseline imaging sessions prior to noise exposure (**Fig. 3A**). On Day 0, approximately 30-60 min hours after noise exposure, CCol growth functions were greatly reduced. Interestingly, approximately 24 hours after noise exposure (Day 1), CCol growth functions had returned to baseline despite a significant ongoing shift in DPOAE and ABR thresholds (Fig 2C-D). On Day 2-4, CCol growth functions were potentiated above baseline before settling at baseline by Day 5, despite the permanent loss of cochlear afferent synapses and reduced ABR wave 1 amplitude.

Following hearing loss, the paradoxical increase in sound-evoked responses in the auditory CNS is described as an increased "central gain" because, unlike a constant "DC" shift in the responses across sound levels, there is an increase in the multiplicative scaling term that describes the growth in neural response per unit step in sound pressure level. Increased scaling of growth functions through central gain can be demonstrated directly by plotting the mean

sound-evoked CCol response amplitude on Day -2 against each subsequent day. The slope of the linear fit represents the response gain, where slopes <1 and >1 represent the divisive and multiplicative terms, respectively, that reflect the transformation in response between the two imaging sessions. Plotting the same data shown in Fig. 3A in this manner reveals no change in gain before noise exposure, strong divisive gain hours after noise exposure, and a transient potentiation in CCol gain several days later (**Fig. 3B**).

A similar pattern of CCol gain changes were noted in each mouse that we tested: Sound-evoked CCol responses were scaled down immediately following noise exposure, but were transiently increased above baseline for several days following noise exposure before returning close to baseline (**Fig 4A,** Repeated measures ANOVA, main effect for gain change across imaging sessions, $F = 5.59$; $p < 0.0005$). Importantly, all mice showed compensation or over-compensation in CCol responses on Day 1, when substantial shifts in cochlear and ABR response thresholds were noted (Fig. 2A). Because the precise timing of potentiated CCol gain varied between individual mice (area of the curve above the gray dashed line in Fig. 4A), we operationally defined the "Days after" epoch as the day within Day 1-3 with the maximal gain. We observed a significant decrease in CCol gain 30-60 min after noise exposure, significantly increased central gain several days after noise exposure (a period when cochlear response thresholds were elevated), but no significant change in gain 6 days after noise exposure despite the permanent loss of cochlear afferent synapses (ANOVA post-hoc pairwise comparisons for each post-exposure period relative to baseline, $p < 0.05$ after Bonferroni-Holm correction for multiple comparisons, **Fig. 4B**).

Discussion

Due to intense noise exposure or the normal effects of aging, sensory and non-sensory cells in the inner ear degenerate over time, reducing the strength and precision of afferent signals conveyed to auditory processing centers in the brain. In response to decreased afferent drive from the auditory periphery, adult auditory CNS circuits increase central gain, which serves to enhance neural excitability through a wide range of intrinsic, presynaptic, post-synaptic and network-level changes[15]. In contrast to the precise homeostatic adjustment described here in CCol population responses, central gain potentiation measured in other cell types often 'over-shoots the mark', elevating central excitability above baseline levels at all stages of auditory processing – from the cochlear nucleus to the cortex -, which has been linked to hyper-synchronization, dysrhythmia and associated perceptual disorders including hyperacusis and tinnitus[47,48]. Understanding the contributions of central auditory gain to auditory processing and perception is challenging in cases of widespread cochlear damage, because the loss of outer hair cell-based amplification introduces complex changes in cochlear tuning that are inextricable from changes arising through central plasticity. For this reason, isolating the effects of increased central gain on auditory response properties *in vivo* is more readily achieved through hearing loss protocols that selectively eliminate cochlear afferent neurons in the spiral ganglion (cochlear afferent neuropathy) or their peripheral synapses onto inner hair cells (cochlear afferent synaptopathy) without inducing changes (or inducing only temporary changes) to cochlear transduction and amplification mechanisms.

Central gain enhancement in auditory cortex is titrated by the extent of cochlear afferent damage

Selective lesions of cochlear afferent neurons or their distal synapses onto inner hair cells engages central gain mechanisms that compensate for the loss of peripheral afferent drive and restore neural coding for basic sound features and behavioral detection thresholds[42,49–53]. The degree of recovered central auditory processing through enhanced central gain is dependent upon the degree of cochlear afferent loss. Near-complete bilateral lesions of cochlear afferent neurons (> 97%) may be beyond the limits of recovery through central gain, as sound-evoked activity in the central pathway was absent and animals showed no behavioral evidence of hearing[42]. Interestingly, slightly less extreme bilateral cochlear neuropathy (90-95% loss) still eliminated early waves of the ABR and brainstem-based auditory reflexes, yet approximately half of treated mice gradually recovered sound-evoked responses in ACtx over a 4-6 week period[14,42]. Unilateral elimination of 90-95% of cochlear afferent neurons was associated with far more robust recovery of ACtx sound processing than bilateral afferent lesions; sound-evoked cortical responses through the denervated ear recovered or exceeded baseline responsiveness and normal sound detection behavior was observed in nearly all subjects[42,54]. Substantial, but less extreme, bilateral inner hair cell afferent lesions distributed across the cochlear frequency map (40-85%) has also been associated with a progressive increase in sound-evoked ACtx responses over 5-14 days that eventually exceeded control levels and enabled a complete recovery of sound detection thresholds[15,51,55].

Hierarchical regulation of central gain following selective afferent lesions

Enhanced central gain and functional recovery following selective cochlear afferent lesions is more rapid and robust at higher stages of central processing. At the level of the auditory nerve compound action potential, sound-evoked response amplitudes directly report the extent of cochlear afferent loss with no observable regulation of gain[15,42,46,55,56]. Similarly, measurements of brainstem far-field evoked potentials and brainstem acoustic reflexes show minimal gain enhancement at the earliest stations of central auditory processing following selective cochlear afferent lesions[42,57,58], though some studies have reported enhanced acoustic startle and medial olivocochlear reflexes after a moderate presumed loss of cochlear afferent synapses[59,60]. Enhanced central gain in the IC following moderate afferent lesions supports a near-complete recovery of unit response thresholds and sound-evoked response rates, although central gain enhancement is slower to develop and less robust overall than ACtx[14,55,61,62]. Following more extreme cochlear afferent neuropathy, sound-evoked responsiveness and auditory decoding accuracy in the IC did not fully recover, even when auditory responsiveness in simultaneously recorded ACtx neurons recovered to – or even surpassed – normative control levels[42]. Gain enhancement in the medial geniculate body of the auditory thalamus (MGB) following selective afferent lesions is intermediate to the compensatory plasticity described in the ACtx and IC; auditory growth functions show near-complete recovery following profound unilateral cochlear denervation[54] and even surpass control responses following moderate synaptopathy, particularly in animals with behavioral evidence of tinnitus[63].

Cortical circuits supporting enhanced central gain following synaptopathy

Contemporary approaches for *in vivo* neural circuit dissection are beginning to shed light on the coordinated set of changes that emerge across cortical cell types following cochlear afferent lesions. In a recent study that used the same moderate intensity noise exposure described here, ACtx single unit response thresholds were elevated and firing rates evoked by high-frequency tones were suppressed over a 3-5-day period following noise exposure[14]. Receptive field tuning and overall responsiveness to low-frequency tones, corresponding to intact regions of the cochlear apex, rose above baseline levels over a 1-3-week period following noise exposure. Importantly, the strength of intracortical inhibition mediated by fast-spiking parvalbumin-expressing GABAergic neurons was decreased within hours following the end of noise exposure, was maximally depressed approximately 1 week following noise exposure and only returned to 80% of its original strength over the following month.

Based on the combination of enhanced sound-evoked responses in the auditory thalamus[63], reduced intracortical inhibition, the competitive invasion of low-frequency cortical map inputs and enhanced cortical responses to low-frequency tones, we expected that the net excitatory output of the cortical column would be potentiated above baseline for at least 1 week following noise exposure. In fact, our earlier work showing enhanced central gain following more extreme unilateral cochlear neuropathy suggested that the net responsiveness across the cortical column was enhanced for 1 month after afferent loss, and perhaps longer[42]. The present work tests these predictions by using a broadband noise token to measure the net population response from CCol neurons, a major output pathway from the ACtx. To our surprise, CCol gain was only enhanced for the first few days following noise exposure before stabilizing at baseline levels (Fig. 4). The time course of this change fits the signature of a

homeostatic plasticity process; a loss of afferent input induces *i)* a brief dip in responsiveness that *ii)* is fully compensated within 24 hours, but then *iii)* briefly overshoots the mark, causing a rebound in responsiveness beyond baseline levels before *iv)* resettling on the baseline homeostatic set point within several days[64].

In other cell types, the prolonged time course of gain enhancement and the persistent elevation above baseline levels is not a homeostatic process, strictly speaking. That the response gain of corticofugal output neurons is regulated more rapidly and precisely than other cortical cell types has interesting implications for the circuit-level mechanisms that implement enhanced central gain. The complete homeostatic regulation of auditory responsiveness in excitatory, glutamatergic CCol neurons may also explain why central gain enhancement in the IC following cochlear afferent lesions do not exceed normative response levels[42,55,61,65].

Behavioral consequences of corticofugal gain control

Innate behaviors are directly enabled by low-level circuits in the brainstem and midbrain. However, even the simplest behavior does not occur in isolation, but rather can be modulated by short-term stimulus history or long-term memories of prior experience. Recent evidence suggests that descending corticofugal neurons in the auditory and visual cortex are optimally positioned to provide an essential source of contextual modulation for innate behaviors because they are embedded in highly plastic centers for sensory processing yet project to midbrain and brainstem circuits that drive innate behaviors such as escape, arrest as well as various sensorimotor reflexes[36,37,66–68].

Subcortical circuits that encode low-level stimulus features to enable coordinated sensorimotor behaviors must also adapt to large-scale shifts in afferent drive resulting from sensory deprivation or damage to sensory end organs. Corticofugal projections from auditory and visual cortex may play a key role in these forms of behavioral adaptation as well. For example, CCol projections are necessary for experience-dependent recovery of sound localization accuracy following unilateral auditory deprivation[32,69] and corticofugal projections from the visual cortex support the recovery of adaptive eye tracking reflexes following damage to the vestibular end organ[70]. In this context, homeostatic adjustments in the auditory response gain of CCol neurons reported here may provide an essential descending input to stabilize auditory coding in midbrain circuits in an early period following cochlear injury. Future work will reveal how the plasticity of auditory corticofugal projection neurons described here is coordinated with pre- and post-synaptic gain changes to shape adaptive and maladaptive changes in auditory perception following peripheral damage.

Methods

All procedures were approved by the Massachusetts Eye and Ear Infirmary Animal Care and Use Committee and followed the guidelines established by the National Institute of Health for the care and use of laboratory animals.

Chronic imaging preparation

Virus injection: Adult CBA/CaJ mice aged 6-8 weeks of either sex (N=5) were anesthetized using isoflurane in oxygen (5% induction; 1.5-2% maintenance) with core body temperature maintained at 36.5°. Glass capillary pipettes tips were inserted 0.5mm into the auditory cortex via two small craniotomies (0.5-1mm diameter) atop presumed caudal and rostral regions of the auditory cortex. We then injected 250 nl of AAV5.Syn.GCaMP6s.WPRE.SV40 (UPENN Vector Core) into each craniotomy at 15 nl/min using an automated injection system (Stoelting). The wound was closed and an analgesic administered (Buprenex, 0.05 mg/kg and Meloxicam, 0.1 mg/kg) before placing animals in a warmed recovery chamber.

Chronic imaging preparation

Cranial windows: Glass cover slips were first etched in piranha solution (H_2O_2 mixed with H_2SO_4 in a 3:1 ratio) and stored in 70% ethanol. A 4mm diameter cover slip was centered and affixed to a 3mm cover slip (#1 thickness, Warner Instruments) using a transparent, UV-cured adhesive (Norland Products). Windows were stored in double deionized water and rinsed with sterile saline before use.

Cranial window surgery: Animals were anesthetized with isoflurane in oxygen (5% induction; 1.5-2% maintenance) and an intraperitoneal 2mg/kg of dexamethasone sodium phosphate was administered to reduce brain edema. After removing the periosteum from the dorsal surface of the skull, an etchant (C&B Metabond) was applied for 30 sec to create a better adhesive surface. A custom titanium headplate (iMaterialise) was bonded to the dorsal surface of the skull with dental cement (C&B Metabond). A 3mm circular craniotomy was made in the

skull overlying the IC with a pneumatic dental drill and diamond bur (head diameter 1/10 mm, NeoDiamond – Microcopy Dental). Once liberated, the bone flap was removed with great care and irrigated constantly with saline so as to avoid rupturing the large pia vessels underneath. The cranial window was then lowered into place using a 3-D manipulator and bonded to the surrounding regions of the skull. Post-operative injections of Buprenex (0.05 mg/kg) and Meloxicam (0.1 mg/kg) were administered and the mice were allowed to recover in a warmed chamber.

Widefield transcranial imaging

Imaging was performed in awake, head-fixed mice inside of a light- and sound-attenuating chamber mounted to an isolated optical table (Thorlabs). Blue light illumination was supplied in epifluorescence configuration from a broadband arc lamp (Lumen Dynamics) passed through a filter cube housing an [Excitation band = 482 ± 9 nm] excitation filter, [Reflection band: 350 – 488 nm; Transmission band: 502 – 950 nm] dichroic mirror and [Emission band = 520 ± 14 nm] emission filter (Thorlabs) and focused on the surface of the IC with a 4X/0.25 NA objective (Nikon). Images (1392 x 1040 pixels) were acquired with a 1.4 Megapixel CCD camera and transferred to a PC via a Gigabit Ethernet interface to a framegrabber PCI card (Thorlabs). Image acquisition was hardware-triggered at 10 frames/s using a TTL pulse train synched to stimulus generation.

Stimulus presentation

Stimuli were generated with a 24-bit digital-to-analog converter (National Instruments model PXI 4461) and presented via a free-field tweeter (Vifa) positioned 10 cm from the left (contralateral) ear canal. Stimuli were calibrated before recording with a wideband ultrasonic acoustic sensor (Knowles Acoustics, model SPM0204UD5). Broadband noise bursts (50 ms duration, 4 ms raised cosine onset/offset ramps) were pseudorandomly presented between 20-80 dB SPL in 10 dB increments (50 repetitions per stimulus). Trial duration was 2 sec.

Imaging data analysis

Original images were first downsampled by a factor of 4 using bicubic interpolation. A region of interest (ROI) was positioned over an IC region with maximum CCol fluorescence that did not include surface blood vessels. Exact ROI dimensions varied between mice depending on blood vessel patterns (100 x 100 ± 50 pixels), but did not vary in size or position between imaging sessions. Population GCaMP responses were obtained from the mean of all pixels within the ROI.

We first computed a fractional change in fluorescence (F) relative to the first frame (F_0), to account for non-stationarities in the GCaMP6 signal within and between the imaging session(s). This $\Delta F/F_0$ was then averaged across all trials for each stimulus presentation. Finally, a response amplitude (%) was computed by subtracting the pre-stimulus baseline from the peak of the post-stimulus response. Further, a linear model was used to regress the response amplitudes on each day to the response amplitudes on Day -2. The slope of this least-squares fit was used to quantify sensory gain.

Acoustic Overexposure

The acoustic overexposure stimulus was an octave band of noise (8-16 kHz) presented at 100 dB SPL for 2 hrs. During exposures, animals were awake and unrestrained within a 12 x 16 x 16 cm, acoustically transparent cage. The cage was suspended directly below the horn of the sound-delivery loudspeaker in a reverberant chamber. Noise calibration to target SPL was performed immediately before each exposure session.

Cochlear Function Tests

Mice were anesthetized with ketamine and xylazine (100/10 mg/kg for ketamine/xylazine, respectively, with boosters of 50 mg/kg ketamine given as needed). Core body temperature was maintained at 36.5° with a homeothermic blanket system. Acoustic stimuli were presented via in-ear acoustic assemblies consisting of two miniature dynamic earphones (CUI CDMG15008–03A) and an electret condenser microphone (Knowles FG-23339-PO7) coupled to a probe tube. Stimuli were calibrated in the ear canal in each mouse before recording. ABR stimuli were 5 ms tone pips (8, 11.3, 16, 22.6 and 32 kHz pure tones) with a 0.5 ms rise-fall time delivered at 27 Hz. Intensity was incremented in 5 dB steps, from 20-80 dB SPL. ABR threshold was defined as the lowest stimulus level at which a repeatable waveform could be identified. DPOAEs were measured in the ear canal using primary tones with a frequency ratio of 1.2, with the level of the f2 primary set to be 10 dB less than f1 level, incremented together in 5 dB steps. The 2f1-f2 DPOAE amplitude and surrounding noise floor were extracted. DPOAE threshold was defined as the lowest of at least two continuous f_2 levels for which the DPOAE amplitude was at least 2 standard deviations greater than the noise floor. All

treated animals underwent rounds of DPOAE and ABR testing before, 2 days and approximately 14 days after noise exposure.

Post-mortem microscopy

Mice were deeply anesthetized with isoflurane and prepared for transcardial perfusion. They were perfused with 0.01 M phosphate buffered saline (pH = 7.4) followed by 4% paraformaldehyde in 0.01 M PBS. Brains were then removed and stored in 4% paraformadehyde for 12 hrs before transferring to cryoprotectant (30% sucrose) for at least 48 hrs. Sections (40 mm thick) were cut using a cryostat (Leica), mounted on glass slides and coverslipped using Vectashield Mounting Medium with DAPI (Vector Labs). The position and size of the infection zone and distribution of CCol axons was visualized and photographed using a Leica epifluorescence microscope (Leica).

Statistical analyses

All statistical analyses were performed in Matlab (Mathworks). Repeated measures ANOVAs were used to compare physiological measurements over dependent variables such as days of measurement in the same group of animals. Post-hoc pairwise multiple comparisons were corrected with Bonferroni-Holm.

Acknowledgements

We thank the GENIE Program, the Janelia Farm Research Campus, and Penn Vector Core in the Gene Therapy Program of the University of Pennsylvania for providing the GCaMP6s reagents

for this project. We thank Ed Hight for designing the head fixation hardware. We thank J. Dahmen for guidance on the corticocollicular imaging preparation. This work was supported by NIDCD R01 DC009836 (D.B.P), NIDCD F32 DC015376 (R.S.W.) and a Herchel Smith Graduate fellowship (M.A.)

References

1. Guinan Jr, J. J. Olivocochlear efferents: anatomy, physiology, function, and the measurement of efferent effects in humans. *Ear Hear.* **27,** 589–607 (2006).
2. Robinson, B. L. & McAlpine, D. Gain control mechanisms in the auditory pathway. *Curr. Opin. Neurobiol.* **19,** 402–407 (2009).
3. Willmore, B. D. B., Cooke, J. E. & King, A. J. Hearing in noisy environments: noise invariance and contrast gain control. *J. Physiol.* **592,** 3371–3381 (2014).
4. Turrigiano, G. Homeostatic synaptic plasticity: local and global mechanisms for stabilizing neuronal function. *Cold Spring Harb. Perspect. Biol.* **4,** a005736–a005736 (2012).
5. Yang, S., Su, W. & Bao, S. Long-term, but not transient, threshold shifts alter the morphology and increase the excitability of cortical pyramidal neurons. *J. Neurophysiol.* **108,** 1567–1574 (2012).
6. Li, S., Kalappa, B. I. & Tzounopoulos, T. Noise-induced plasticity of KCNQ2/3 and HCN channels underlies vulnerability and resilience to tinnitus. *eLife* **4,** 1–23 (2015).
7. Yang, S., Weiner, B. D., Zhang, L. S., Cho, S.-J. & Bao, S. Homeostatic plasticity drives tinnitus perception in an animal model. *Proc. Natl. Acad. Sci.* **108,** 14974–14979 (2011).
8. Kalappa, B. I., Anderson, C. T., Goldberg, J. M., Lippard, S. J. & Tzounopoulos, T. AMPA receptor inhibition by synaptically released zinc. *Proc Natl Acad Sci U S A* **112,** 15749–54 (2015).
9. Sarro, E. C., Kotak, V. C., Sanes, D. H. & Aoki, C. Hearing loss alters the subcellular distribution of presynaptic GAD and postsynaptic GABAA receptors in the auditory cortex. *Cereb. Cortex* **18,** 2855–2867 (2008).
10. Kotak, V. C. *et al.* Hearing loss raises excitability in the auditory cortex. *J. Neurosci.* **25,** 3908–18 (2005).
11. Takesian, A. E., Kotak, V. C. & Sanes, D. H. Presynaptic GABAB Receptors Regulate Experience-Dependent Development of Inhibitory Short-Term Plasticity. *J. Neurosci.* **30,** 2716–2727 (2010).
12. Yang, S., Weiner, B. D., Zhang, L. S., Cho, S.-J. & Bao, S. Homeostatic plasticity drives tinnitus perception in an animal model. *Proc. Natl. Acad. Sci. U. S. A.* **108,** 14974–9 (2011).
13. Middleton, J. W. *et al.* Mice with behavioral evidence of tinnitus exhibit dorsal cochlear nucleus hyperactivity because of decreased GABAergic inhibition. *Proc. Natl. Acad. Sci. U. S. A.* **108,** 7601–6 (2011).
14. Resnik, J. & Polley, D. B. Fast-spiking GABA circuit dynamics in the auditory cortex predict recovery of sensory processing following peripheral nerve damage. *eLife* **6,** (2017).
15. Salvi, R. *et al.* Inner hair cell loss disrupts hearing and cochlear function leading to sensory deprivation and enhanced central auditory gain. *Frontiers in Neuroscience* **10,** (2017).
16. Terreros, G. & Delano, P. H. Corticofugal modulation of peripheral auditory responses. *Front. Syst. Neurosci.* **9,** 1–8 (2015).
17. Winer, J. A. Decoding the auditory corticofugal systems. *Hear. Res.* **207,** 1–9 (2005).
18. Stebbings, K. A., Lesicko, A. M. H. & Llano, D. A. The auditory corticocollicular system: Molecular and circuit-level considerations. *Hear. Res.* **314,** 51–59 (2014).

19. Diamond, I. T., Jones, E. G. & Powell, T. P. S. The projection of the auditory cortex upon the diencephalon and brain stem in the cat. *Brain Res.* **15,** 305–340 (1969).
20. Lesicko, A. M. H. & Llano, D. A. Impact of peripheral hearing loss on top-down auditory processing. *Hear. Res.* **343,** 4–13 (2017).
21. Robinson, B. L., Harper, N. S. & McAlpine, D. Meta-adaptation in the auditory midbrain under cortical influence. *Nat. Commun.* **7,** 13442 (2016).
22. Malmierca, M. S., Anderson, L. A. & Antunes, F. M. The cortical modulation of stimulus-specific adaptation in the auditory midbrain and thalamus : a potential neuronal correlate for predictive coding. **9,** 1–14 (2015).
23. Winkowski, D. E. & Knudsen, E. I. Top-down gain control of the auditory space map by gaze control circuitry in the barn owl. *Nature* **439,** 336–339 (2006).
24. Suga, N. & Ma, X. Multiparametric corticofugal modulation and plasticity in the auditory system. *Nat. Rev. Neurosci.* **4,** 783–794 (2003).
25. Nakamoto, K. T., Jones, S. J. & Palmer, A. R. Descending projections From auditory cortex modulate sensitivity in the midbrain to cues for spatial position. *J. Neurophysiol.* **99,** 2347–2356 (2008).
26. Slater, B. J., Willis, A. M. & Llano, D. A. Evidence for layer-specific differences in auditory corticocollicular neurons. *Neuroscience* **229,** 144–154 (2013).
27. Llano, D. A. & Sherman, S. M. Differences in Intrinsic Properties and Local Network Connectivity of Identified Layer 5 and Layer 6 Adult Mouse Auditory Corticothalamic Neurons Support a Dual Corticothalamic Projection Hypothesis. *Cereb. Cortex* **19,** 2810–2826 (2009).
28. Rock, C. & Apicella, A. j. Callosal Projections Drive Neuronal-Specific Responses in the Mouse Auditory Cortex. *J. Neurosci.* **35,** 6703–6713 (2015).
29. Joshi, A., Kalappa, B. I., Anderson, C. T. & Tzounopoulos, T. Cell-Specific Cholinergic Modulation of Excitability of Layer 5B Principal Neurons in Mouse Auditory Cortex. *J. Neurosci.* **36,** 8487–8499 (2016).
30. Sun, Y. J., Kim, Y. J., Ibrahim, L. A., Tao, H. W. & Zhang, L. I. Synaptic Mechanisms Underlying Functional Dichotomy between Intrinsic-Bursting and Regular-Spiking Neurons in Auditory Cortical Layer 5. *J. Neurosci.* **33,** 5326–5339 (2013).
31. Harris, K. D. & Mrsic-flogel, T. D. Cortical connectivity and sensory coding. *Nature* **503,** 51–58 (2013).
32. Bajo, V. M., Nodal, F. R., Moore, D. R. & King, A. J. The descending corticocollicular pathway mediates learning-induced auditory plasticity. *Nat. Neurosci.* **13,** 253–260 (2010).
33. Homma, X. N. Y. *et al.* A Role for Auditory Corticothalamic Feedback in the Perception of Complex Sounds. *J. Neurosci.* **37,** 6149–6161 (2017).
34. Torii, M., Hackett, T. A., Rakic, P., Levitt, P. & Polley, D. B. EphA Signaling Impacts Development of Topographic Connectivity in Auditory Corticofugal Systems. *Cereb. Cortex* **23,** 775–785 (2013).
35. Guo, W. *et al.* A corticothalamic circuit for dynamic switching between feature detection and discrimination. *Neuron* **in press,** 1–15 (2017).
36. Zingg, B. *et al.* AAV-mediated anterograde transsynaptic tagging: mapping corticocollicular input-defined neural pathways for defense behaviors. *Neuron* **93,** 33–47

(2017).
37. Xiong, X. R. *et al.* Auditory cortex controls sound-driven innate defense behaviour through corticofugal projections to inferior colliculus. *Nat. Commun.* **6,** 7224 (2015).
38. Znamenskiy, P. & Zador, A. M. Corticostriatal neurons in auditory cortex drive decisions during auditory discrimination. *Nature* **497,** 482–485 (2013).
39. Barnstedt, O., Keating, P., Weissenberger, Y., King, A. J. & Dahmen, J. C. Functional microarchitecture of the mouse dorsal inferior colliculus revealed through In vivo two-photon calcium imaging. *J. Neurosci.* **35,** 10927–39 (2015).
40. Wekselblatt, J. B., Flister, E. D., Piscopo, D. M. & Niell, C. M. Large-scale imaging of cortical dynamics during sensory perception and behavior. *J. Neurophysiol.* **115,** 2852–2866 (2016).
41. Chen, T.-W. *et al.* Ultrasensitive fluorescent proteins for imaging neuronal activity. *Nature* **499,** 295–300 (2013).
42. Chambers, A. R. *et al.* Central gain restores auditory processing following near-complete cochlear denervation. *Neuron* **89,** 1–13 (2016).
43. Kujawa, S. G. & Liberman, M. C. Adding insult to injury: cochlear nerve degeneration after 'temporary' noise-induced hearing loss. *J. Neurosci.* **29,** 14077–14085 (2009).
44. Liberman, M. C. & Kujawa, S. G. Cochlear synaptopathy in acquired sensorineural hearing loss: Manifestations and mechanisms. *Hear. Res.* **349,** 138–147 (2016).
45. Sergeyenko, Y., Lall, K., Liberman, M. C. & Kujawa, S. G. Age-related cochlear synaptopathy: an early-onset contributor to auditory functional decline. *J. Neurosci.* **33,** 13686–13694 (2013).
46. Yuan, Y. *et al.* Ouabain-induced cochlear nerve degeneration: synaptic loss and plasticity in a mouse model of auditory neuropathy. *J. Assoc. Res. Otolaryngol.* **15,** 31–43 (2013).
47. Auerbach, B. D., Rodrigues, P. V & Salvi, R. J. Central gain control in tinnitus and hyperacusis. *Front. Neurol.* **5,** (2014).
48. Roberts, L. E. *et al.* Ringing Ears: The Neuroscience of Tinnitus. *J. Neurosci.* **30,** 14972–14979 (2010).
49. Zeng, F. G. Perceptual consequences of disrupted auditory nerve activity. *J. Neurophysiol.* **93,** 3050–3063 (2005).
50. Kraus, N. *et al.* Consequences of neural asynchrony: a case of auditory neuropathy. *J. Assoc. Res. Otolaryngol.* **1,** 33–45 (2000).
51. Lobarinas, E., Salvi, R. & Ding, D. Insensitivity of the audiogram to carboplatin induced inner hair cell loss in chinchillas. *Hear. Res.* 1–8 (2013).
52. Starr, A., Picton, T. W., Sininger, Y., Hood, L. J. & Berlin, C. I. Auditory neuropathy. *Brain* **119 (Pt 3,** 741–53 (1996).
53. Schuknecht, H. F. & Woellner, R. C. Hearing losses following partial section of the cochlear nerve. *Laryngoscope* **63,** 441–65 (1953).
54. Chambers, A. R., Salazar, J. J. & Polley, D. B. Persistent thalamic sound processing despite profound cochlear denervation. *Front. Neural Circuits* **10,** 1–13 (2016).
55. Qiu, C., Salvi, R., Ding, D. & Burkard, R. Inner hair cell loss leads to enhanced response amplitudes in auditory cortex of unanesthetized chinchillas: evidence for increased system gain. *Hear. Res.* **139,** 153–171 (2000).
56. Lobarinas, E., Spankovich, C. & Le Prell, C. G. Evidence of 'hidden hearing loss' following

noise exposures that produce robust TTS and ABR wave-I amplitude reductions. *Hear. Res.* **349,** 155–163 (2016).

57. Valero, M. D., Hancock, K. E. & Liberman, M. C. The middle ear muscle reflex in the diagnosis of cochlear neuropathy. *Hear. Res.* **332,** 29–38 (2016).
58. Shaheen, L. A., Valero, M. D. & Liberman, M. C. Towards a Diagnosis of Cochlear Neuropathy with Envelope Following Responses. *J. Assoc. Res. Otolaryngol.* **745,** 727–745 (2015).
59. Knudson, X. I. M., Shera, C. A. & Melcher, J. R. Increased contralateral suppression of otoacoustic emissions indicates a hyperresponsive medial olivocochlear system in humans with tinnitus and hyperacusis. *J Neurophysiol* **112,** 3197–3208 (2014).
60. Hickox, A. E. & Liberman, M. C. Is noise-induced cochlear neuropathy key to the generation of hyperacusis or tinnitus? *J. Neurophysiol.* **111,** 552–564 (2014).
61. Wake, M., Takeno, S., Mount, R. J. & Harrison, R. V. Recording from the inferior colliculus following cochlear inner hair cell damage. *Acta Otolaryngol.* **116,** 714–720 (1996).
62. Boyen, K., de Kleine, E., van Dijk, P. & Langers, D. R. M. Tinnitus-related dissociation between cortical and subcortical neural activity in humans with mild to moderate sensorineural hearing loss. *Hear. Res.* **312,** 48–59 (2014).
63. Kalappa, B. I., Brozoski, T. J., Turner, J. G. & Caspary, D. M. Single unit hyperactivity and bursting in the auditory thalamus of awake rats directly correlates with behavioural evidence of tinnitus. *J. Physiol.* **592,** 5065–78 (2014).
64. Hengen, K. B., Lambo, M. E., Van Hooser, S. D., Katz, D. B. & Turrigiano, G. G. Firing rate homeostasis in visual cortex of freely behaving rodents. *Neuron* **80,** 335–342 (2013).
65. Möhrle, D. *et al.* Loss of auditory sensitivity from inner hair cell synaptopathy can be centrally compensated in the young but not old brain. *Neurobiol. Aging* **44,** 173–184 (2016).
66. Aizenberg, M., Mwilambwe-Tshilobo, L., Briguglio, J. J., Natan, R. G. & Geffen, M. N. Bidirectional Regulation of Innate and Learned Behaviors That Rely on Frequency Discrimination by Cortical Inhibitory Neurons. *PLOS Biol.* **13,** e1002308 (2015).
67. Aizenberg, M. & Geffen, M. N. Bidirectional effects of aversive learning on perceptual acuity are mediated by the sensory cortex. *Nat. Neurosci.* **16,** 994–996 (2013).
68. Liang, F. *et al.* Sensory cortical control of a visually induced arrest behavior via corticotectal projections. *Neuron* **86,** 755–767 (2015).
69. Nodal, F. R., Bajo, V. M. & King, A. J. Plasticity of spatial hearing: behavioural effects of cortical inactivation. *J. Physiol.* **590,** 3965–86 (2012).
70. Liu, B., Huberman, A. D. & Scanziani, M. Cortico-fugal output from visual cortex promotes plasticity of innate motor behaviour. *Nature* **538,** 383–387 (2016).

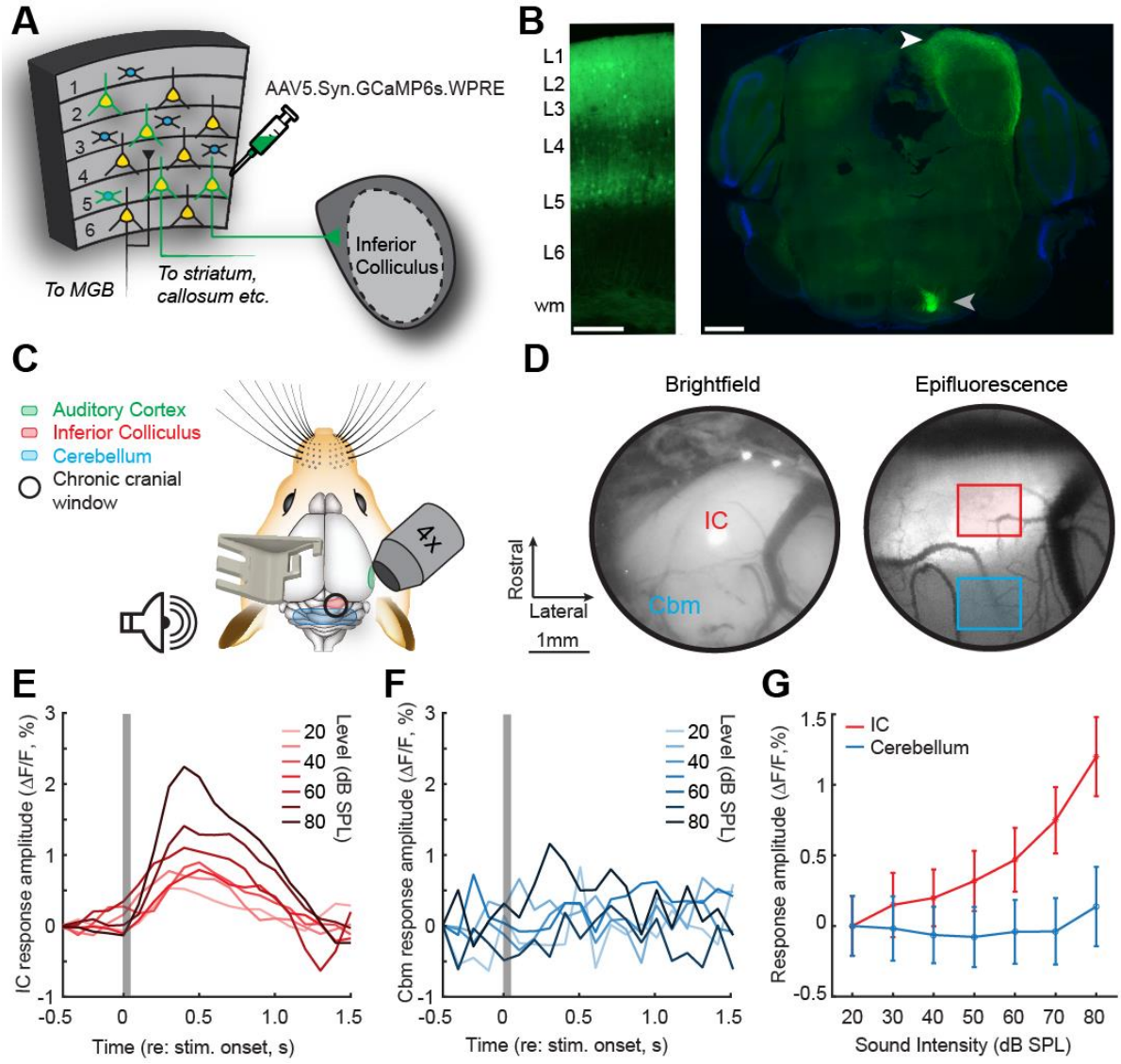

Figure 1. Imaging sound-evoked activity in auditory corticocollicular axon terminals. (**A**) The genetically encoded calcium indicator, GCaMP6s, was expressed in a heterogeneous set of inhibitory (blue) and excitatory (yellow) neurons in ACtx. (**B**) *Left*, a post-mortem coronal section of the ACtx reveals GCaMP6s expression in neurons in all layers (L) though, whether because of the injection depth (0.5 mm, L5) or due to viral vector tropism, expression was strongest in L5 pyramidal neurons somata, their apical dendrites in L2/3 and their axon terminals in the white matter (wm). *Right*, a coronal section through the inferior colliculus (IC) shows a halo of GCaMP6s-labeled ACtx axon terminals in the dorsal and external cortex of the IC ipsilateral to the injection site that would be accessible to surface imaging techniques (white arrowhead). ACtx axon terminals are also observed in the brainstem, where they innervate the superior olivary complex (gray arrowhead) and dorsal cochlear nucleus. (**C**) A preparation for chronic imaging of sound-evoked activity in ACtx corticocollicular (CCol) axons from awake, head-fixed mice. (**D**) The dorsal surface of the IC and cerebellum (Cbm) as seen through the implanted cranial window with brightfield (left) and epifluorescent (right) illumination. Note the

difference in fluorescence between the IC and Cbm. Red and blue rectangles represent regions of interest (ROIs) used for measurements of sound-evoked activity. (**E-F**) The time course of mean GCaMP6s activity evoked by broadband noise bursts of varying intensity from ROIs in the IC (E) and Cbm (F). Gray boxes denote stimulus timing and duration. (**G**) Monotonic growth of CCol peak response amplitudes across sound levels. Data represent mean ± SEM.

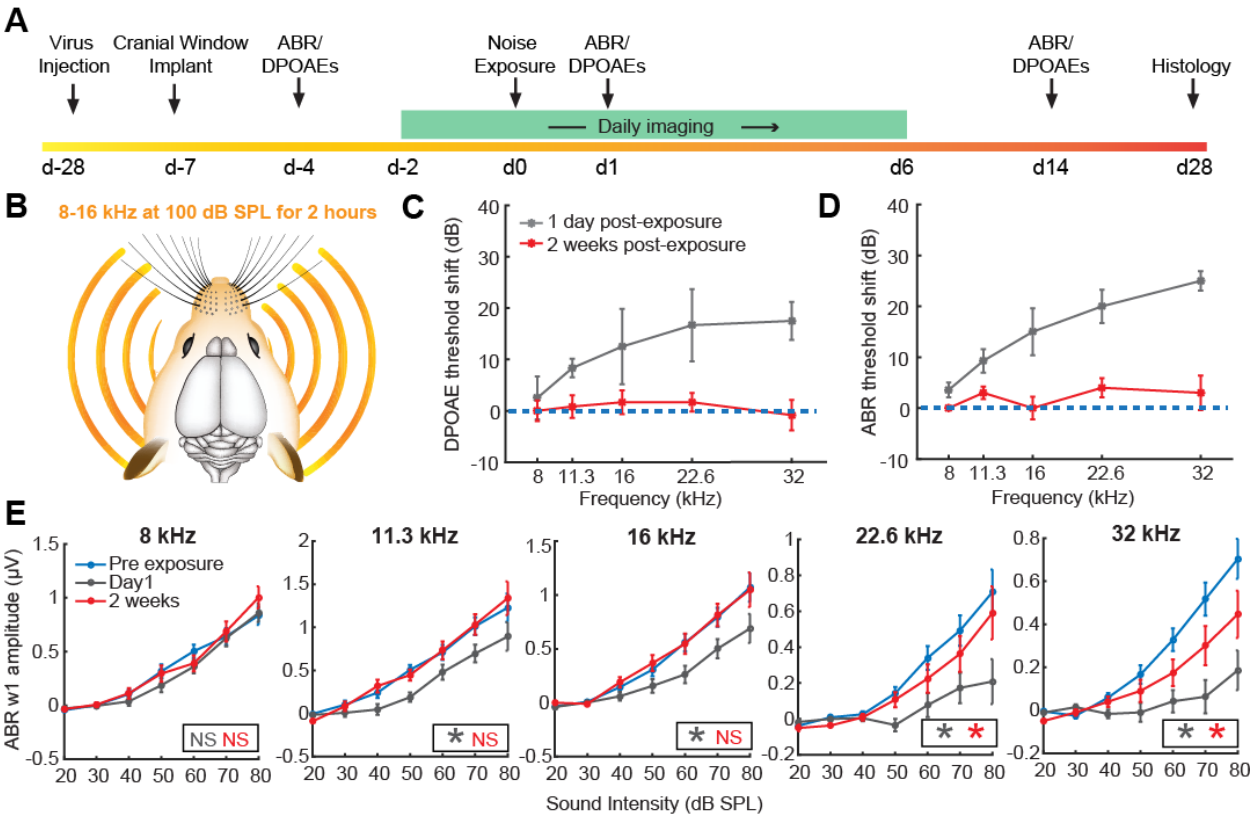

Figure 2. Moderate intensity noise exposure induces a temporary shift in cochlear and brainstem response thresholds but a permanent loss of auditory nerve afferent fibers. (**A**) Timing of all procedures used in a single mouse to measure changes in CCol axon responses before and after noise exposure. (**B**) Noise exposure protocol. (**C-D**) Elevations in distortion product otoacoustic emission (DPOAE) and auditory brainstem response (ABR) thresholds (*C* and *D*, respectively) are observed 1 day following noise exposure (gray) but have returned to baseline 2 weeks following noise exposure (red). (**E**) The growth of ABR wave 1 (w1) across sound levels is shown at 3 measurement times for 5 sound frequencies. Note that the persistent loss of w1 amplitudes at high test frequencies is known to arise from the permanent loss of cochlear nerve afferent synapses onto inner hair cells in the high-frequency base of the cochlea. NS = no significant difference with pre-exposure. Asterisk = significant main effect for ABR amplitude between pre-exposure and post-exposure. Gray = Day 1 vs pre-exposure; Red = 2 weeks vs pre-exposure. Data represent mean ± SEM.

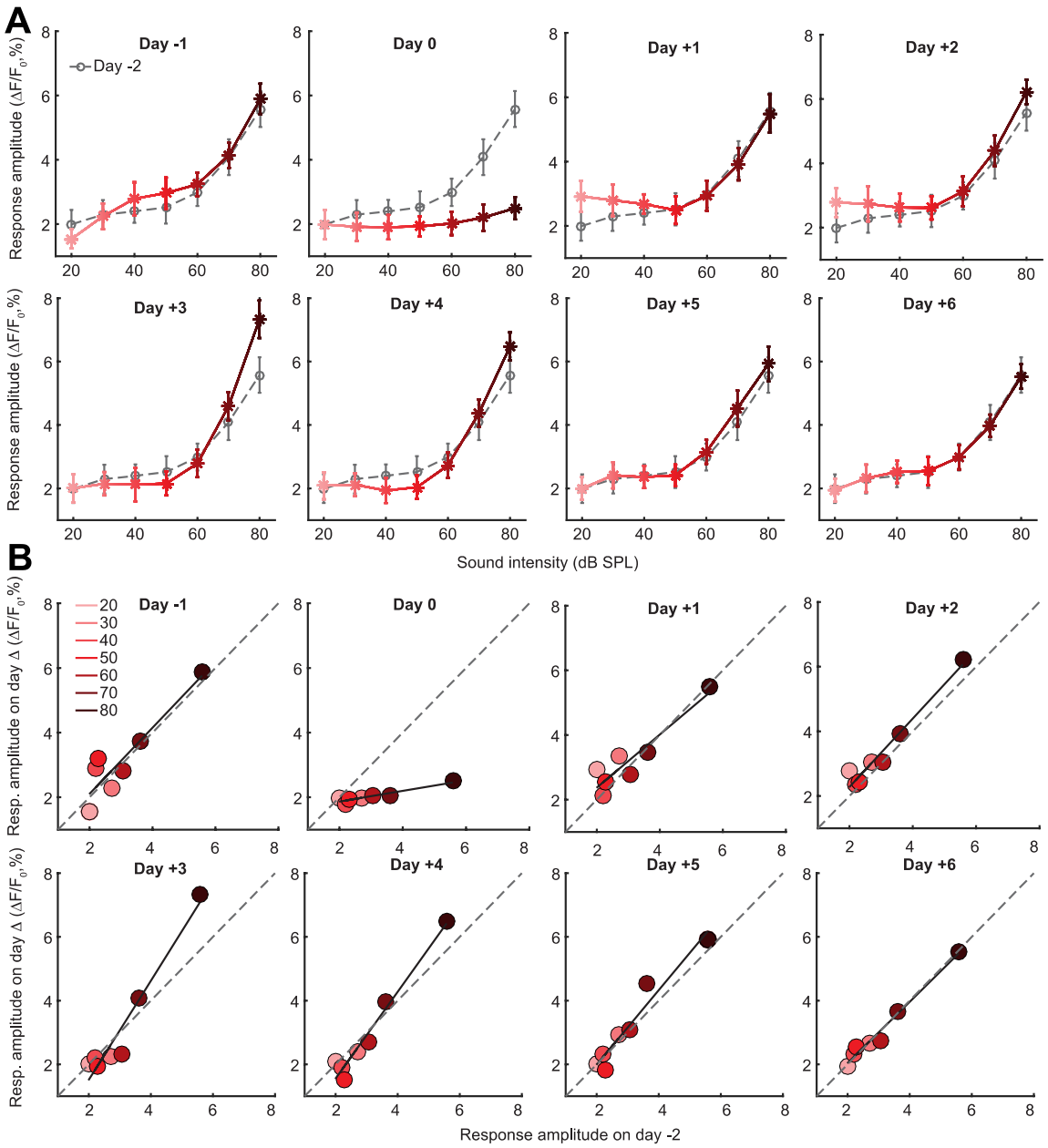

Figure 3. Rapid scaling of corticocollicular response gain in the first days following noise exposure. (**A**) Daily changes in CCol response growth across sound intensities from a single mouse relative to the day of noise exposure (Day 0). The first imaging session was performed 2 days prior to noise exposure and serves as a reference for subsequent days (Day -2, dashed gray lines). Day 0 imaging was performed 30-60 min after noise exposure ended. Data represent mean peak amplitude ± SEM. (**B**) Scatterplots of the peak response data from the same mouse with superimposed linear fits. Linear fits with slope > 1 and < 1 reflect multiplicative and divisive scaling of the response gain, respectively (where the dashed diagonal line represents no change in response slope). Note divisive scaling hours following noise exposure, followed by multiplicative scaling several days after noise and then a return to baseline by Day +6.

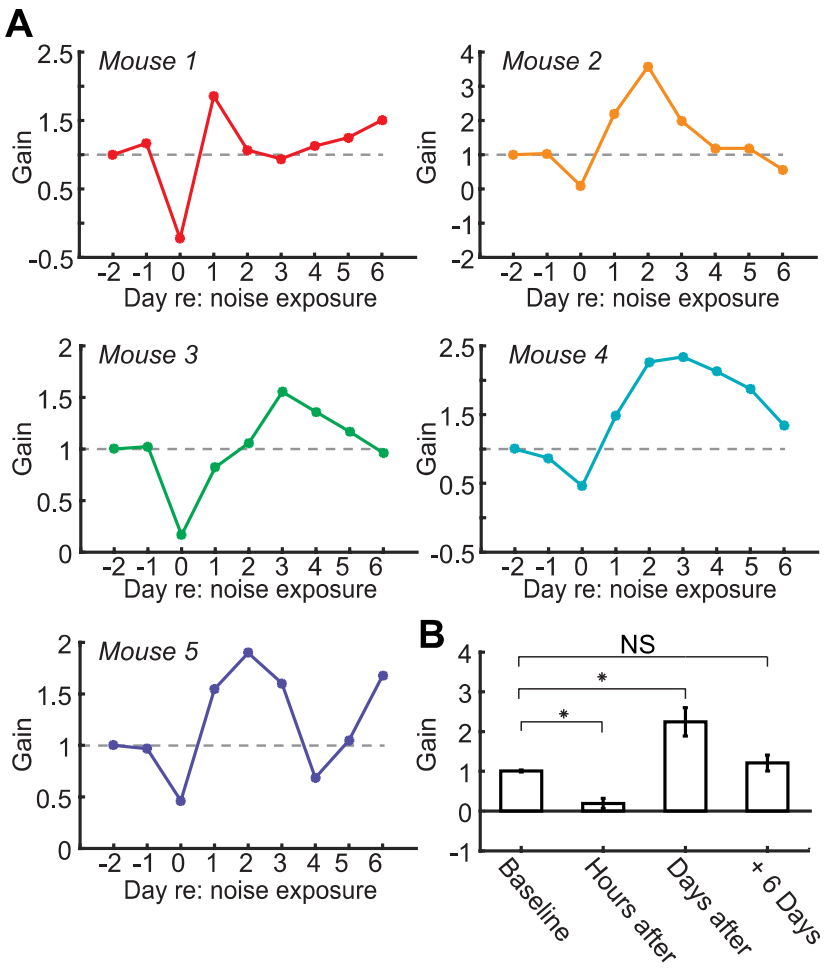

Figure 4. Rapid normalization of corticocollicular response gain within several days following noise exposure. (**A**) Daily changes in CCol response gain for each mouse tested in this study. CCol gain was computed as the slope term of the linear fit equation for any given day referenced to Day -2. Dashed gray line represents a Gain = 1, where there is no change in the slope term relative to Day -2. (**B**) Mean ± SEM gain change in Baseline, day of noise exposure, peak gain change in 1-3 days following noise exposure (days after), and at the final test on Day 6. Asterisks represent $p < 0.05$ in pairwise post-hoc tests after correcting for multiple comparisons. NS = not significant. Data represent mean ± SEM.